



## Review

## Redox flow cells for energy conversion

C. Ponce de León<sup>a,\*</sup>, A. Frías-Ferrer<sup>b</sup>, J. González-García<sup>b</sup>,  
D.A. Szánto<sup>c</sup>, F.C. Walsh<sup>a</sup>

<sup>a</sup> *Electrochemical Engineering Group, School of Engineering Sciences, University of Southampton,  
Highfield, Southampton SO17 1BJ, UK*

<sup>b</sup> *Applied Electrochemistry Group, Department of Physical Chemistry, University of Alicante,  
Ap. Correos 99, 03080 Alicante, Spain*

<sup>c</sup> *National Wind Power, Reading Bridge House, Reading, RG1 8LS, UK*

Received 19 October 2005; received in revised form 10 February 2006; accepted 22 February 2006

## Abstract

Energy storage technologies provide an alternative solution to the problem of balancing power generation and power consumption. Redox flow cells are designed to convert and store electrical energy into chemical energy and release it in a controlled fashion when required. Many redox couples and cell designs have been evaluated. In this paper, redox flow systems are compared in the light of characteristics such as open circuit potential, power density, energy efficiency and charge-discharge behaviour. The key advantages and disadvantages of redox flow cells are considered while areas for further research are highlighted.

© 2006 Published by Elsevier B.V.

**Keywords:** Electrochemical power; Energy storage; Redox flow cells; Regenerative fuel cells

## Contents

|  |    |
|--|----|
| 1. Introduction .....                                | 00 |
| 2. Properties of redox flow cells .....              | 00 |
| 2.1. Characteristics .....                           | 00 |
| 2.2. Reactive species and electrode properties ..... | 00 |
| 2.3. Membrane considerations .....                   | 00 |
| 2.4. Design considerations .....                     | 00 |
| 3. Types of redox fuel cells .....                   | 00 |
| 3.1. Bromine/polysulphide redox battery .....        | 00 |
| 3.2. All vanadium redox battery (VRB) .....          | 00 |
| 3.3. The vanadium-bromine redox system .....         | 00 |
| 3.4. The iron-chromium redox system .....            | 00 |
| 3.5. Zinc/bromine redox flow cells .....             | 00 |
| 3.6. Zinc/cerium redox flow cells .....              | 00 |
| 3.7. Soluble lead-acid battery (undivided) .....     | 00 |
| 4. Other characteristics and comparisons .....       | 00 |
| 5. Summary and further work .....                    | 00 |
| References .....                                     | 00 |

\* Corresponding author.

E-mail address: [capla@soton.ac.uk](mailto:capla@soton.ac.uk) (C. Ponce de León).

## 1. Introduction

The relatively new technologies able to store large quantities of energy have the potential to increase the flexibility of power systems and improve the response to a sudden demand of energy minimising environmental damage. The use of energy storage technologies provides some advantages to electric power transmission systems such as; effective use of existing plant investment, flexibility in operation and better response to price changes. Stored electricity can be made readily available to meet immediate changes in demand allowing effective operation of base load units at high and essentially constant levels of power. An energy storage facility that responds quickly and efficiently to provide or store energy over a wide range of loads could displace less-efficient and more-expensive facilities. Energy storage systems have additional benefits by using off-peak power for pumping and/or charging, maximising operations and flexibility for buying or selling electricity during on-peak or off-peak periods.

Battery technologies can be distinguished in the way energy is stored; lead-acid cells, store energy within the electrode structure whereas redox flow cells systems store the energy in the reduced and oxidised species that recirculate through the cell. Fuel cells, on the other hand, store energy in the reactants externally to the cell. Table 1 provides a comparison among these three systems. Table 2 shows other strategies for energy storage and their main characteristics.

The advantages and disadvantages of conventional, developmental and redox flow cell systems are listed in Table 3. The main electrochemical storage systems at present are the flooded lead-acid battery, the oxygen-recombinant valve-regulated lead-acid (VRLA) battery and redox flow cells. These systems are briefly

described below, followed by a review of redox flow cells storage systems.

Flooded lead-acid batteries [1,2] are by far the most developed technology used for large scale electrochemical energy conversion in the transport industry. These batteries have a long life span and good reliability under extreme working conditions. Their limitations include the relatively frequent maintenance required to replace the water lost during operation, high cost compared to other non-storage options and their heavy weight. These limitations reduce their profitability and transport flexibility. Oxygen-recombinant valve-regulated lead-acid (VRLA) batteries [1,2] use the same technology as flooded lead-acid batteries, but the acid electrolyte is immobilised by sealing the battery with a valve. This eliminates the need for addition of water and avoids electrolyte mix preventing stratification. The oxygen recombination catalyst and the valves of VRLAs prevent venting hydrogen gas and the entrance of air into the cells. VRLA batteries are significantly more-expensive than flooded lead-acid batteries and their expected life span is shorter. The major advantage of VRLAs over flooded lead-acid batteries is the low maintenance necessary to keep the battery in operation. Also, VRLA cells are smaller than flooded cells, reducing the size and weight of the battery.

The advantages of redox flow cells can be summarised in four features: moderate cost, modularity, transportability and flexible operation. Due to their modular design its construction and maintenance costs could be the lowest of any of the storage systems mentioned above. The redox flow batteries are well-suited for transmission and distribution deferral applications, where batteries might be transported from substation to substation or load centre in order to provide local capacity needed to defer expensive upgrades. The modular nature of these batteries simplifies

Table 1  
General comparison of static battery, redox flow cells and fuel cells

| Electrochemical device | Site of reactants/products         | Electrolyte conditions   | Separator                                   |
|------------------------|------------------------------------|--|---|
| Static battery         | Active electrode material          | Static and held within cell                                    | Microporous polymer separator               |
| Redox flow cell        | Aqueous electrolytes in reservoirs | Electrolyte recycles through the cell                          | Ion exchange membrane (cationic or anionic) |
| Fuel cell              | Gaseous or liquid fuel plus air    | Solid polymer or ceramic acts as solid electrolyte within cell | Ion exchange membrane polymer or ceramic    |

Table 2  
Strategies for energy storage

| Energy storage system           | Type of process   | Features  |
|---------------------------------|---|---|
| Compressed air                  | In this technology energy is stored as compressed air and can be withdraw by a combustion turbine-generator   | Special terrain required                                    |
| Pumped hydro                    | In this technology, water is pumped up into a reservoir during off-peak hours; the water generates electricity by gravity through a reversible turbine-generator during on-peak hours | Special terrain required                                    |
| Redox systems (batteries)       | This technology refers to the conversion of electrical energy into chemical that can be recovered by reversing the electrochemical reaction   | No special requirements                                     |
| Superconducting magnetic energy | In this technology, electricity is stored on a superconductor material and is discharged directly as dc power   | Very low temperatures required                              |
| Flywheels                       | This technology stores electricity into kinetics energy and can be taken back by an electrical generator  | Vacuum is required Newer technology Large maintenance costs |

Table 3  
Advantages and disadvantages of storage systems compared to redox flow cells

| Battery energy storage system | Advantages   | Disadvantages  | Redox system  |
|-------------------------------|--|--|---|
| Conventional systems          | Well-known technology<br>Low maintenance<br>Low size   | Frequent maintenance<br>Heavy<br>High construction cost<br>Expensive technology<br>Short life span<br>Not portable | Flooded lead-acid battery<br>Valve-regulated lead-acid (VRLA)                                     |
| Developmental systems         | Transportability<br>High energy (charging) efficiency<br>Flexible operation                        | Thermal management<br>Difficult maintenance  | Sodium/sulfur battery<br>Zinc/bromine redox flow cell   |
| Redox flow cells              | Low cost<br>Modularity<br>Transportability<br>Flexible operation<br>High efficiency<br>Large scale | Newer technology   | Bromine/polysulphide redox flow cell<br>Vanadium redox flow cell<br>Iron/chromium redox flow cell |

their maintenance which can be done separately by individual battery modules.

A major advantage is their flexibility during charge/discharge cycles; the batteries can be discharged completely without damaging the cells, a decided advantage over the lead-acid technologies. Table 4 summarises the main advantages and disadvantages between a conventional lead-acid battery and the most studied redox flow cell, the all vanadium–vanadium system [3].

## 2. Properties of redox flow cells

### 2.1. Characteristics

Redox flow cell energy storage systems are being developed for use in stand-alone village power applications and distributed energy installations for electric utility services. In the former application, either solar photovoltaic arrays [4] or wind turbines supply the primary power and an electrochemical system stores energy during times of excess of power generation and delivers

energy during times of insufficient power generation. Electric utilities can use distributed energy storage on a daily or weekly cycles to provide a load levelling capability for large central power station plants. Life cycle costs, simplicity of operation, flexibility, complexity and state of the technology are among the factors that determine the selection of systems for storage applications.

Energy storage has been identified as a strong requirement for remote power systems. Lead-acid batteries can be used for these applications but as mentioned above, are expensive and not easy to maintain, while the redox flow cell storage systems appears to be a more viable option [5]. Redox energy storage systems possess features such as flexible design, long life and high reliability with acceptable operation and maintenance costs. Redox flow cell storage systems use two soluble redox couple as electroactive species that are oxidised or reduced to store or deliver energy. In the divided mode, the electrodes are separated by an ion exchange membrane while the reactants contained in separate storage tanks are recirculated through the redox flow

Table 4  
Characteristics of lead-acid battery compared with the all vanadium redox system, adapted from Ref. [3]

| Lead-acid battery (deep cycle)  | Vanadium redox flow cell   |
|---|--|
| Storage efficiency 70–80% depending on age  | Storage efficiency expected to reach 90% under favourable, low current density conditions                      |
| Storage capacity and power rating are interrelated by chemical energy storage in the electrodes         | Non-participating electrodes allow storage capacity and power rating to be designed independently              |
| Battery voltage varies 10% between charged and discharged states  | Voltage is constant through charging and discharging processes   |
| Easily damaged by excessive charge or discharge   | No damage from complete discharge; but overcharging must be prevented  |
| Can only be charged slowly  | Can be charged at any rate by electric current or by replacing the electrolytes                                |
| Damaged by rapid discharging  | Can be discharged at any rate  |
| Lifetime reduced by microcycles (rapid fluctuations in charging rate as in wind and solar applications) | Not affected by microcycles  |
| Requires regular maintenance  | Very low maintenance is expected   |
| Life rarely exceeds five years (because phase changes deteriorate electrodes)                           | Life expected to be at least 20 years (no phase changes in the battery and use of durable membrane technology) |
| Cost and size of battery per kilowatt is constant as storage capacity increases                         | Cost per kilowatt decreases as storage capacity increases and size is smaller than lead-acid battery           |

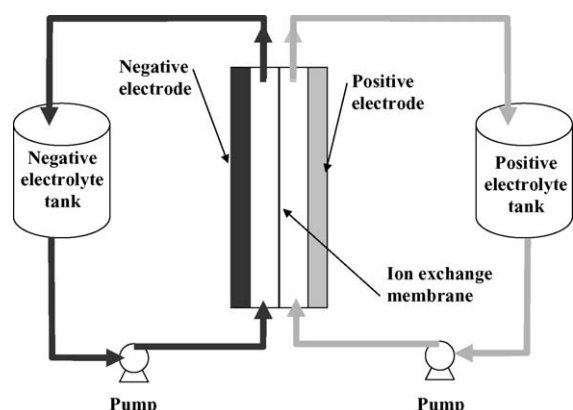


Fig. 1. Unit redox flow cell for energy storage.

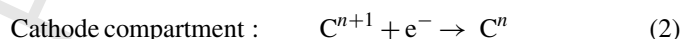
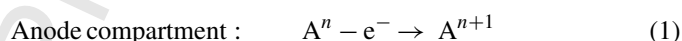
of the electrolyte. Both energy and power can be easily varied from just a few hours (as in emergency uninterruptible power supplies or load-levelling applications) to several days or weeks (as needed for remote area stand-alone applications employing photovoltaic or wind generating systems).

## 2.2. Reactive species and electrode properties

The electrode reactions must be reversible and both the oxidised and reduced species must be soluble with their redox potential as far apart as possible. The cost of reactants must be reasonable and the electrolytes must be chemically stable and easy to prepare at high concentrations.

## 2.3. Membrane considerations

The membrane must reduce the transport of reactive species between the anode and cathode compartments to a minimum rate and to allow the transport of non-reactive species and water to maintain electroneutrality and electrolyte balance. In a typical redox cell system such as



the membrane should be an impermeable barrier for A and C ions in both states of charge. Typical strategies are proton transport in acid electrolytes or  $\text{Na}^+$  transport in the presence of sodium salts. Other considerations include: low electric resistivity, long life span, easy manufacture and handling and moderate cost.

## 2.4. Design considerations

Major challenges to the development of redox flow batteries include:

- Shunt (bypass or leakage) currents [6]: these self-discharge currents of the electrolyte are best reduced by increasing the ionic resistance of the flow ports by making the length of the manifold longer or by reducing the cross-sectional area of the ports. However, increasing the manifold length of the cell ports increases the electrolyte flow resistance demanding more pumping power complicating cell design and increasing costs. A compromise must be reached between the energy saved by reducing the shunt currents and the additional energy needed to recirculate the electrolyte.
- Flow distribution in the stack [7]: ideally, the face of each electrode should “see” a constant mean linear flow electrolyte velocity (typically  $0.1\text{--}10\text{ ms}^{-1}$ ) in a plug flow electrolyte regime. In practice, uneven flow distribution occurs and stagnant zones are formed in certain areas of the electrode surface.
- Reactant back mixing: partially depleted reactant leaves the cell and return to their respective tanks mixing with more concentrated reactant. At any time, the reactants entering the cell are at lower concentration than they would be if the

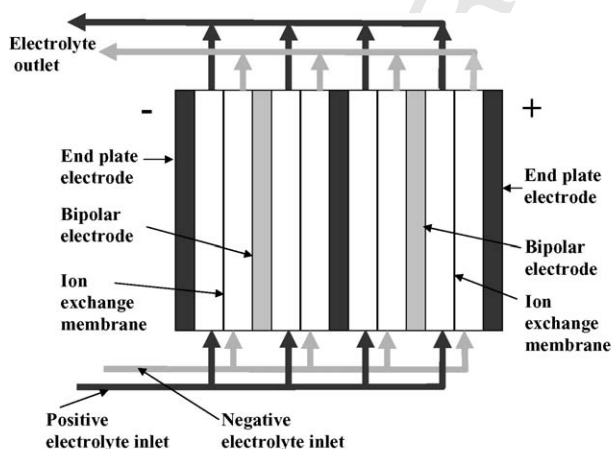


Fig. 2. Stack consisted of four redox flow cells with bipolar electrodes.



mixing had not occurred causing a gradual drop in the cell potential. The problem could be avoided using two tanks for each reactant; one for new reactants going towards the cell and other for depleted reactants coming out from the cell.

- (d) Compensation for ionic migration: the water transferred across the membrane by osmosis or electro-osmosis changes the concentration of ionic species during the operation of the battery. Therefore, the electrolyte must be treated by a suitable method such as reverse osmosis, water evaporation or electrodialysis to remove unwanted formed species and to maintain the redox couple concentrated and pure.

**Figures of merit:** The main figures of merit defined for a redox flow cell systems are: voltage efficiency; the ratio of cell voltage between discharge and charge cycles

$$\eta_V = \frac{V_{cc}(\text{discharge})}{V_{cc}(\text{charge})} \quad (3)$$

where  $V_{cc}$  (discharge) and  $V_{cc}$  (charge) are the discharge and charge cell voltages, respectively at certain time or state of charge during the operation of the cell.

Charge efficiency; the ratio of electrical charge used during discharge compared to that used during charge

$$\eta_C = \frac{Q(\text{discharge})}{Q(\text{charge})} \quad (4)$$

Energy efficiency; the ratio of energy between the discharge and charge processes

$$\eta_e = \frac{E(\text{discharge})}{E(\text{charge})} \quad (5)$$

Power efficiency; the ratio of power between discharge and charge processes

$$\eta_p = \frac{IV_{cc}(\text{discharge})}{IV_{cc}(\text{charge})} \quad (6)$$

It is important to refer these figures of merit to electrolyte volume, reactant conversion, and state of charge as well as considering practical design and operational factors.

### 3. Types of redox fuel cells

#### 3.1. Bromine/polysulphide redox battery

In these batteries, the electrolytes during the discharge cycle are: sodium bromide in the positive side, and sodium polysulphide on the negative side [8–12]. These chemical species are abundant, their cost is reasonable and they are very soluble in aqueous media. During the charging cycle shown in Fig. 3a, the bromide ions are oxidised to bromine and complexed as tribromide ions. The following half-cell reactions are involved: at the positive electrode, bromide ions are transformed to tribromide ions

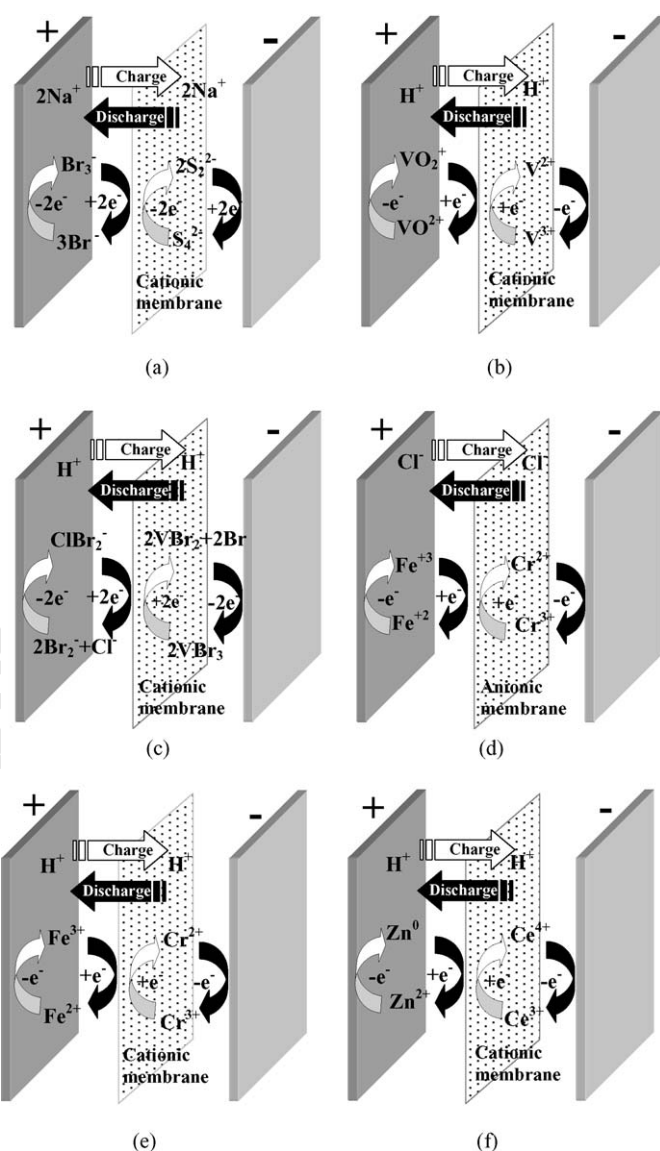
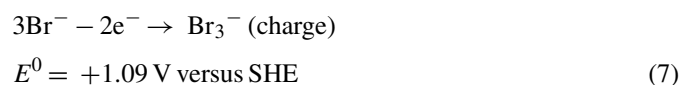
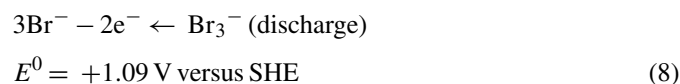
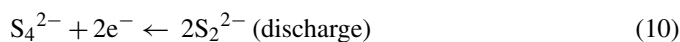
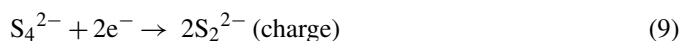


Fig. 3. Redox flow systems: (a) bromine/polysulphide, (b) vanadium/vanadium, (c) vanadium/bromide, (d) iron/chromium with anionic membrane, (e) iron/chromium with cationic membrane, and (f) zinc/bromide.



At the negative electrode the sulfur present as soluble polysulphide anion, is reduced to sulphide ion in the charge cycle; the reactions being simplified to



The electrolyte solutions are separated by a cation selective membrane to prevent the sulfur anions reacting directly with bromine and the electrical balance is achieved by the transport of sodium ions across the membrane. On discharge, the sulphide ion is the reducing agent and the tribromide ion the

Table 5  
Nominal Module Sizes of Regenesys® Cells [12]

| Parameter   | Module series |           |                  |
|---|---------------|-----------|------------------|
|   | S (small)     | L (large) | XL (extra large) |
| Individual electrode cross-sectional area ( $\text{m}^{-2}$ ) | 0.11          | 0.21      | 0.67             |
| Number of bipolar electrodes                                  | <60           | <120      | <200             |
| Total electrode area ( $\text{m}^{-2}$ )                      | <6.6          | <25       | <134             |

oxidising species. The open circuit cell potential is around 1.5 V and varies depending on the concentration of the electrochemically active species. Challenges with this system include: (a) the nature of the different electrolytes causes cross-contamination of both electrolyte solutions over a period of time, (b) the difficulty in maintaining electrolyte balance, i.e., a fixed composition, (c) the possibility of deposition of sulfur species in the membrane and (d) the need to prevent  $\text{H}_2\text{S}(\text{g})$  and  $\text{Br}_2(\text{g})$  formation.

This system was successfully evaluated by the former Innogy Technologies; Regenesys Ltd. [9,10] in 1 MW test facility. Tables 5 and 6 show the sizes of the modular cells developed by this company and the specifications for the plant constructed at the Little Barford site, respectively. The next step in process

Table 6  
Outline specification planned for the Regenesys® energy storage plant at Little Barford, UK [10]

|                                       |   |
|---------------------------------------|---|
| Overall plant parameters              |   |
| Maximum rated power output            | 15 MW   |
| Energy storage capacity               | 120 MWh   |
| Discharge duty cycle                  | 10 h  |
| Design turnaround efficiency          | 60–65%  |
| Predicted lifetime                    | >15 years                                       |
| Site area                             | <3000 $\text{m}^2$                              |
| Design availability                   | 95%   |
| Power conservation system             |   |
| Power rating                          | 15 MW, 18 MV A                                  |
| Design response time                  | <100 ms   |
| dc link operating voltage             | $\pm 2400$ V                                    |
| Design ramp rate                      | +15 to –15 MW in <100 ms                        |
| Inverter ac output voltage            | 6600 V  |
| Cell parameters                       |   |
| Membrane                              | Nafion® cationic                                |
| Nominal cell voltage                  | 1.5 V   |
| Electrode area                        | 0.67 $\text{m}^2$                               |
| Electrolytes                          | NaBr and NaS (15 $\text{m}^3$ of each per MW h) |
| XL module                             |   |
| Typical number of cells perm stack    | 200   |
| Nominal discharge power rating        | 100 kW  |
| Operating voltage range               | 150–360 V                                       |
| Module open circuit voltage           | 300 V   |
| Module layout                         |   |
| Total number of XL modular stacks     | 120   |
| Number of stacks in electrical series | 12 (each string)                                |
| Number of parallel strings            | 10  |

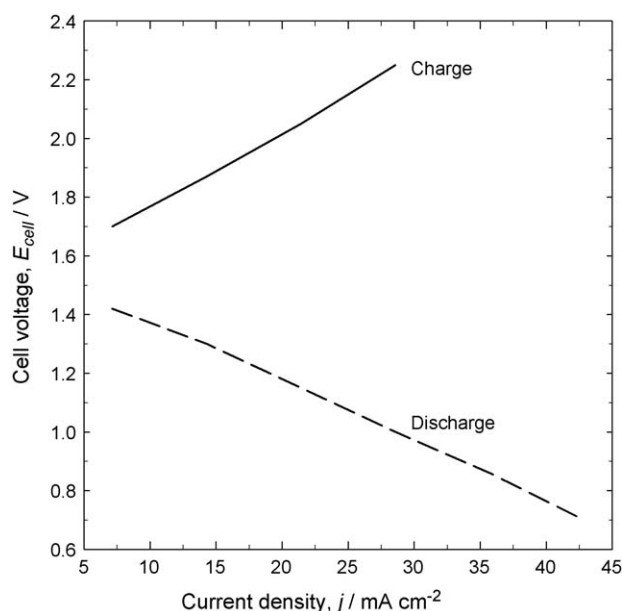


Fig. 4. Cell voltage vs. a range of charge and discharge current densities for a 50% charged sulfur-bromine redox battery. About  $1 \text{ mol dm}^{-3}$  NaBr saturated with  $\text{Br}_2$ , and  $2 \text{ mol dm}^{-3}$   $\text{Na}_2\text{S}$  in contact with a graphite and porous sulphide nickel electrodes, respectively separated by a Nafion® 125 membrane. Electrode area of  $35 \text{ cm}^2$  and  $0.25 \text{ cm}$  interelectrode gap [12].

development was to build a 15 MW h utility scale energy storage plant [13]. A typical 100% charged sulfur-bromine redox battery consist of  $1 \text{ mol dm}^{-3}$  flow-by sodium bromide solution saturated with bromine, in contact with a graphite electrode separated by a Nafion® 125 ion exchange membrane from a  $2 \text{ mol dm}^{-3}$  flow-through  $\text{Na}_2\text{S}$  electrolyte, in contact with a porous sulphide nickel electrode [12]. With an electrode area of  $35 \text{ cm}^2$  and interelectrode gap 100 mils, the open circuit voltage of this redox battery was 1.74 V; the open circuit voltage at 50% charge is 1.5 V. Fig. 4 shows a typical curve of cell voltage versus charge and discharge current densities at 50% state of charge [12].

Fig. 5 shows the overall cell voltage of a monopolar cell with activated carbon/polyolefin pressed electrodes divided by a Nafion® 115 membrane containing  $5 \text{ mol dm}^{-3}$  NaBr as anolyte and  $1.2 \text{ mol dm}^{-3}$   $\text{Na}_2\text{S}$  as a catholyte [14]. During the charging cycle for 30 min at  $40 \text{ mA cm}^{-2}$  the cell voltage climbed sharply from 1.7 to 2.1 V. This behaviour could be explained by the different overpotentials created within the cell and the adsorption of bromine on the activated carbon. During the discharge cycle at the same current, the curve shows a characteristic critical point at which the voltage drops, indicating complete discharge. Activated carbon adsorbs bromine providing readily available reactant and the discharge process only becomes mass transport controlled at high reactant conversion levels. Operation of redox flow cells under deep discharge high fractional conversions conditions necessitates mass transport conditions. Under these circumstances, high electrolyte flow velocity, effective turbulence promoters and roughened electrode surfaces become important factors in achieving a satisfactory performance.

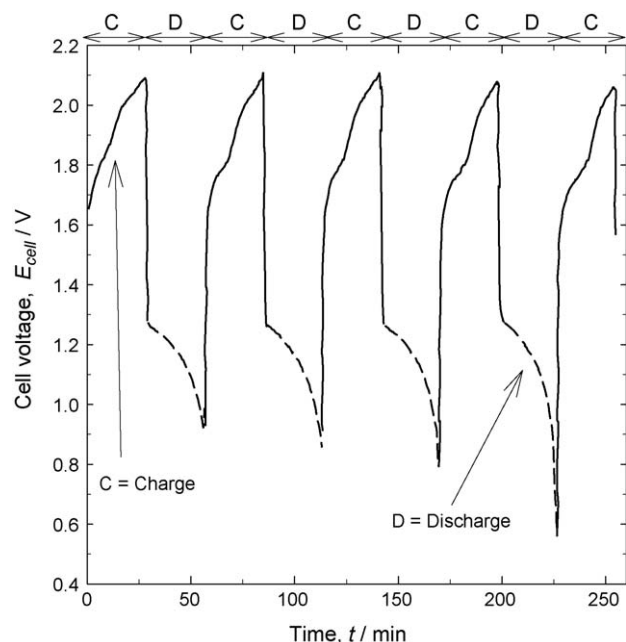


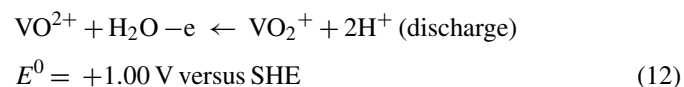
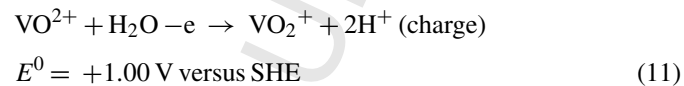
Fig. 5. Cell potential vs. time response during charge/discharge cycles at a current density of  $40 \text{ mA cm}^{-2}$  for a sulfur/bromine monopolar test cell with activated carbon-polyolefin pressed plates as electrode materials [14].

More recently, nickel foam and carbon felt materials separated by a Nafion® 117 cationic membrane were used as negative and positive electrodes, respectively, for bromine/polysulphide redox flow battery [15]. Both electrodes showed good electrocatalytic activity but the internal ohmic resistance of the cell restricted the overall energy efficiency to 77.2%, at current density of  $40 \text{ mA cm}^{-2}$  and cell power density of  $56 \text{ mW cm}^{-2}$ .

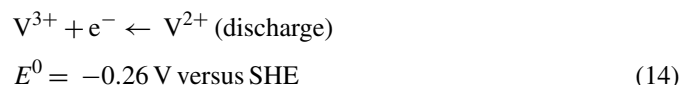
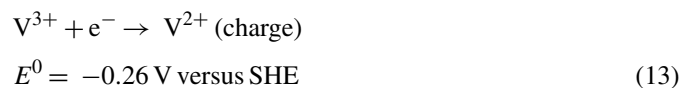
### 3.2. All vanadium redox battery (VRB)

The vanadium redox battery shown in Fig. 3b employs vanadium ions to store energy in both half-cell electrolytes and uses, e.g., graphite felt electrodes [16]. The V(II)/V(III) redox couple is employed at the negative electrode while the positive electrode uses the V(IV)/V(V) redox couple [17,18]. Electrical balance is achieved by the migration of hydrogen ions across a membrane separating the electrolytes. All of the reactants and products of the electrode reactions remain dissolved in one or other of the two electrolytes and, if solution crossover occurs, the vanadium half-cell electrolytes can be remixed and the system brought back to its original state, albeit with a loss of energy efficiency. No significant phase change reactions or electrocrystallization processes occur in the VRB system.

The following half-cell reactions are involved in the all vanadium redox cell. At the positive electrode, vanadium (IV) ions are transformed to vanadium (V) ions



At the negative electrode, vanadium (III) cations are transformed to vanadium (II) cations



Using  $1 \text{ mol dm}^{-3}$  concentrations at  $25^\circ\text{C}$ , the standard open circuit cell potential of this system is 1.26 V. The relatively fast kinetics of the vanadium redox couples allow high coulombic and voltage efficiencies to be obtained but the value of these efficiencies also depends on the internal resistance of the cell.

It is claimed that the VRB is not damaged by fluctuating power demand or by repeated total discharge or charge rates as high as the maximum discharge rates [3,19–29]. It can also be rated to ensure that gassing is eliminated during the high charge rates associated with rapid charging cycles. In addition, VRB cells can be overcharged and overdischarged, within the limits of the capacity of the electrolytes, and can be cycled from any state of charge or discharge, without permanent damage to the cells or electrolytes. There is the problem that the strong activity of a certain kind of vanadium ion, V(V), degrades the ion exchange membrane. Such batteries are being studied in detail by the group of Skyllas-Kazacos at the University of New South Wales [16–40] and by various industrial organisations [3,41].

Fig. 6 shows the second charge and discharge cycles for a cell using vanadium solutions in  $0.5 \text{ mol dm}^{-3} \text{ H}_2\text{SO}_4$  when two dif-

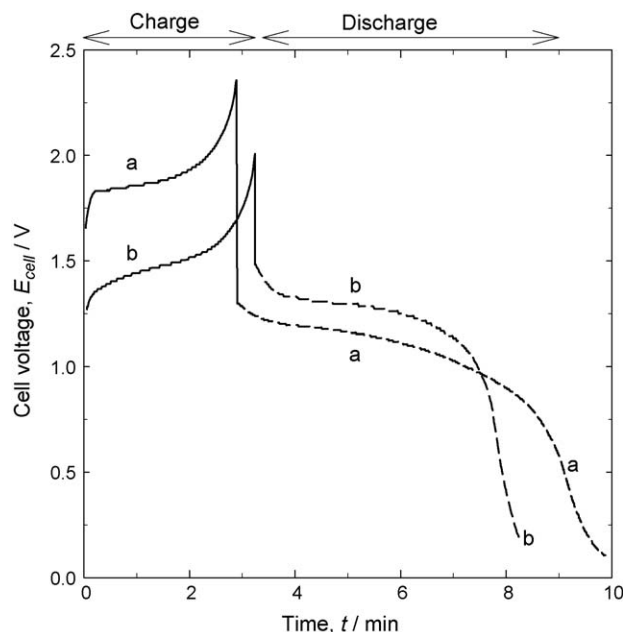


Fig. 6. Charge/discharge responses during the second cycle of a vanadium redox cell with graphite felt electrodes of  $90 \text{ cm}^2$  area: (a)  $0.5 \text{ mol dm}^{-3} \text{ VOSO}_4$  in  $2 \text{ mol dm}^{-3} \text{ H}_2\text{SO}_4$  with a sulfonated polyethylene membrane, charge current density  $15 \text{ mA cm}^{-2}$  and discharge across  $1 \Omega$  resistor (b)  $1.5 \text{ mol dm}^{-3} \text{ VOSO}_4$  in  $2 \text{ mol dm}^{-3} \text{ H}_2\text{SO}_4$  with a polystyrene sulfonic acid membrane, charge current density  $40 \text{ mA cm}^{-2}$ , discharge across  $0.33 \Omega$  resistor. Adapted from Ref. [30].

ferent membranes separated the electrolyte [28]. For a sulfonated polyethylene cation selective membrane in  $0.5 \text{ mol dm}^{-3}$  vanadium solution (charged at  $15 \text{ mA cm}^{-2}$  current density and discharged across  $1 \Omega$  resistor) the open circuit voltage was  $1.47 \text{ V}$  and the coulombic efficiency was  $87\%$ . This indicates a small amount of cross mixing and self-discharge. Better results were obtained when a polystyrene sulfonic acid cation selective membrane was used in a  $1.5 \text{ mol dm}^{-3}$  vanadium electrolyte. The cell was charged at a higher current density of  $40 \text{ mA cm}^{-2}$  and discharged across a  $0.33 \Omega$  resistor to obtain a coulombic and voltage efficiency of  $90\%$  and  $81\%$ , respectively, over  $10\text{--}90\%$  state of charge. The overall energy efficiency with this membrane was  $73\%$  which compares well with most redox flow systems [30].

Fig. 7 shows another example of a charge/discharge curve for an all vanadium redox flow system [25]. The cell consisted of two  $6 \text{ mm}$  thick felt electrodes (of  $132 \text{ cm}^2$  surface area) bonded to a graphite impregnated polyethylene plate (of  $0.26 \text{ mm}$  thickness) separated by a polystyrene sulfonic acid membrane. The electrolyte was  $2 \text{ mol dm}^{-3}$  vanadium sulphate in  $2 \text{ mol dm}^{-3} \text{ H}_2\text{SO}_4$  at  $35^\circ\text{C}$  with a charge/discharge current density of  $30 \text{ mA cm}^{-2}$ . The coulombic, voltage and overall efficiencies at several temperatures for this cell are shown in Fig. 8. The coulombic efficiency decreased slightly with temperature due to vanadium being transported preferentially through the membrane while as expected the voltage efficiency increased slightly with temperature. The combined effect of coulombic and voltage efficiencies produced the highest overall efficiency at  $23^\circ\text{C}$ . The resistance values of the cell during the charge and discharge cycles were  $4.5$  and  $5.4 \Omega \text{ cm}^{-2}$ , respectively, which

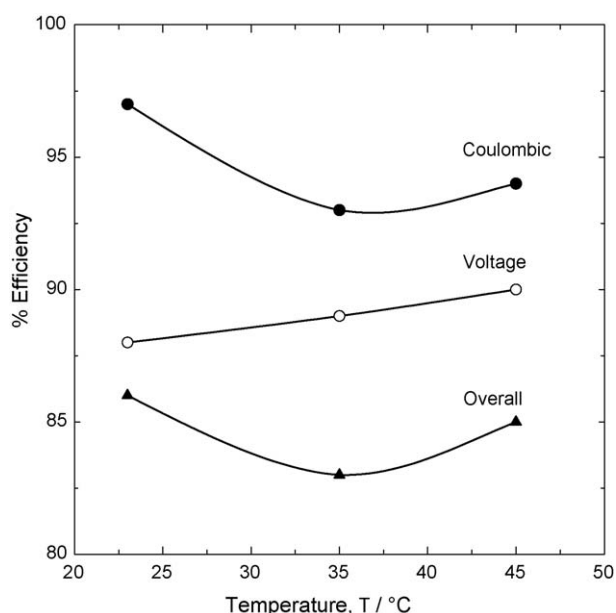


Fig. 8. Performance efficiencies of graphite felt/carbon plastic electrodes at various temperatures for  $2 \text{ mol dm}^{-3}$  vanadium sulphate in  $2 \text{ mol dm}^{-3} \text{ H}_2\text{SO}_4$  redox flow cell: (●) coulombic (○) voltage and (▲) overall. Adapted from Ref. [25].

were obtained from the current potential curves showed in Fig. 9 [25].

A small vanadium redox fuel cell utilising the laminar flow characteristics of two electrolytes operating at very low Reynolds numbers to reduce the convective mixing in a membraneless flow cell has been considered [42]. The two electrolytes containing  $\text{V(V)}/\text{V(IV)}$  and  $\text{V(III)}/\text{V(II)}$ , respectively are stored separately and flow-through the cell generating a

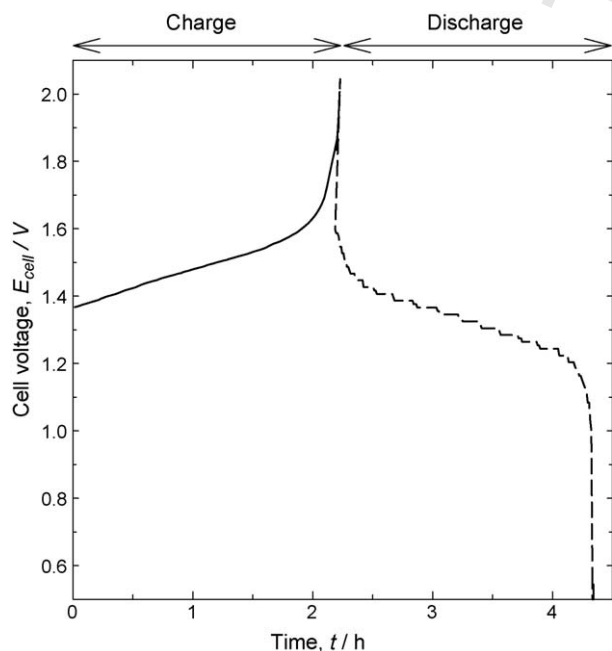


Fig. 7. Charge discharge curve at current density at  $30 \text{ mA cm}^{-2}$  for  $2 \text{ mol dm}^{-3}$  vanadium sulphate in  $2 \text{ mol dm}^{-3} \text{ H}_2\text{SO}_4$  at  $35^\circ\text{C}$  contained in a cell with two  $6 \text{ mm}$  thick felt electrodes of  $132 \text{ cm}^2$  surface area bonded to a graphite impregnated polyethylene plate separated by a polystyrene sulfonic acid membrane [25].

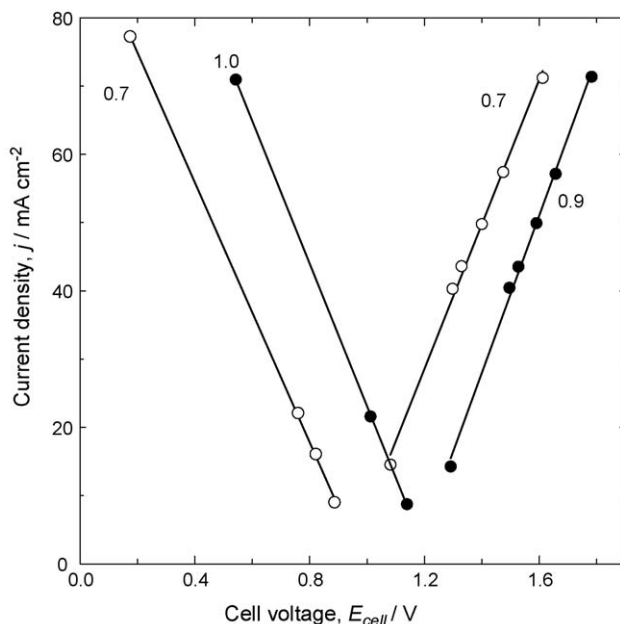


Fig. 9. Current potential curves at  $23^\circ\text{C}$  for a redox flow cell utilizing  $2 \text{ mol dm}^{-3}$  vanadium sulphate in  $2 \text{ mol dm}^{-3} \text{ H}_2\text{SO}_4$ . The numbers on the lines represent the state of charge/discharge of the cell [25].

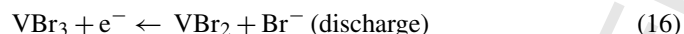


current density of  $35 \text{ mA cm}^{-2}$  at 1.1 V. Although the kinetics of each electrode reactions is rapid, contact between the two electrolyte systems (and very rapid solution redox reaction) drastically reduces the fuel utilization to around 0.1%. The redox fuel cell is interesting from the point of view that eliminates ohmic losses but the very small Reynolds numbers in a laminar fluid flow channel would not be sustainable in larger cell operating at higher Reynolds numbers.

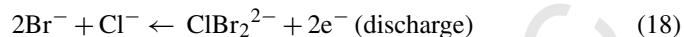
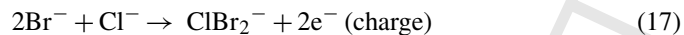
### 3.3. The vanadium-bromine redox system

The all vanadium redox flow cell has a specific energy density of  $25\text{--}35 \text{ Wh kg}^{-1}$  which is considered low for energy vehicle applications [43]. Due to this limitation systems such as vanadium-bromide redox flow cell have long been considered and recently revisited [44,45]. The energy density is related to the concentration of the redox ions in solution, on the cell potential and the number of electrons transferred during the discharge per mol of active redox ions. All vanadium redox flow cells have a maximum vanadium concentration in the region of  $2 \text{ mol dm}^{-3}$ , which limits energy density and represents the solubility limit of V(II) and V(III) ions in sulfuric acid at temperatures from 5 up to  $40^\circ\text{C}$  at which the V(V) ions are still stable.

The vanadium-bromine redox flow cell shown in Fig. 3c employs the  $\text{VBr}_2/\text{VBr}_3$  redox couple at the negative electrode



and the redox couple  $\text{Cl}^-/\text{BrCl}_2^-$  at the positive electrode



Preliminary studies were carried out using  $3\text{--}4 \text{ mol dm}^{-3}$  vanadium-bromide solution by Magnam Technologies [44]. For this concentration of active ions, it is possible to reach energy densities up to  $50 \text{ Wh kg}^{-1}$ .

Fig. 10 shows the charge and discharge time versus the number of cycles of a typical vanadium-bromide redox flow cell at a current of 1 A. The cell contained a Nafion<sup>®</sup> 112 ion exchange membrane separator in an electrolyte consisted of  $3 \text{ mol dm}^{-3}$  V(IV) bromide solution in  $3\text{--}4 \text{ mol dm}^{-3}$  HBr or HBr/HCl on each side of the membrane. The electrodes consisted of carbon or graphite felt bonded onto plastic or conductive plastic sheets [44].

A variation of the vanadium-bromide cell is the vanadium/polyhalide [46] cell in which the polyhalide presents higher oxidation potential and exists as a result of the interaction between halogen molecules and halide ions such as  $\text{Br}_2\text{Cl}^-$  or  $\text{Cl}_2\text{Br}^-$  equivalent to the species  $\text{I}_3^-$  of  $\text{Br}_3^-$ . This system has been tested in a small laboratory scale redox flow cell with two glassy carbon sheets current collectors and graphite felt electrodes separated by a Nafion<sup>®</sup> 112 membrane and  $\text{VCl}_2/\text{VCl}_3$  electrolyte in the negative side and  $\text{Br}^-/\text{ClBr}_2^-$  in the positive side of the cell. At charge/discharge current of  $20 \text{ mA cm}^{-2}$  the cell lead to 83% and 80% coulombic and voltage efficiencies,

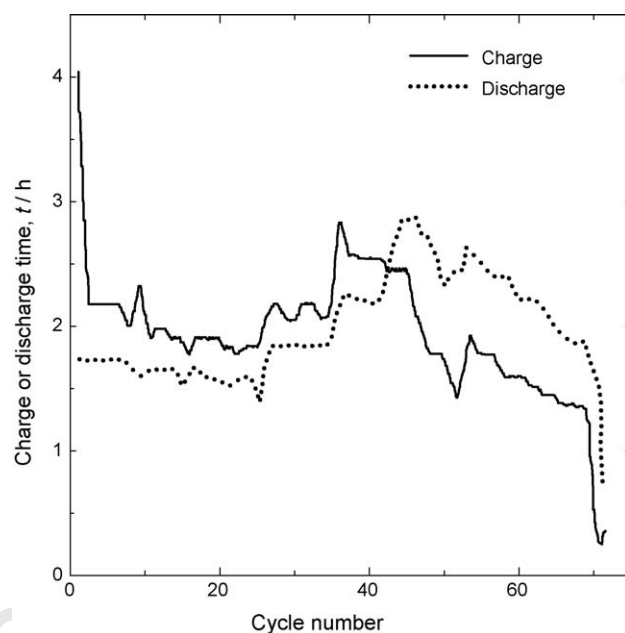


Fig. 10. Charging and discharging time vs. number of cycles for a vanadium-bromide redox flow cell using carbon material bonded to conductive plastic sheets separated by a Nafion<sup>®</sup> 112 cationic membrane. Electrolyte concentration:  $[\text{V}] = 1 \text{ mol dm}^{-3}$ ,  $[\text{Br}^-] = 3 \text{ mol dm}^{-3}$ ,  $[\text{HCl}] = 1.5 \text{ mol dm}^{-3}$ . The charge/discharge current was 1 A. Adapted from Ref. [44].

respectively. Fig. 11 shows the charge/discharge curve for this V/polyhalide redox flow cell. The reactions of this cell are; at the negative electrode

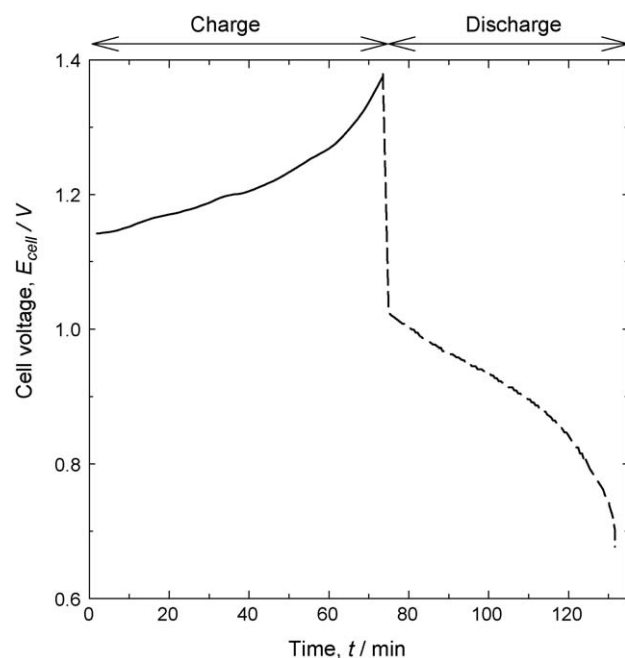
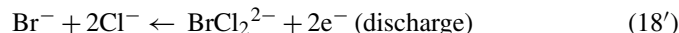
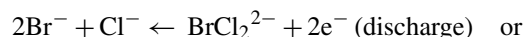
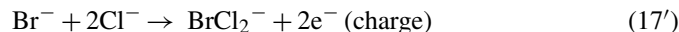
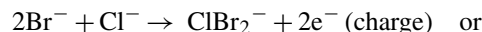


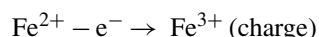
Fig. 11. Charge/discharge response of a vanadium polyhalide redox cell.  $1 \text{ M VCl}_3$  in negative half-cell and  $1 \text{ mol dm}^{-3} \text{ NaBr}$  in positive half-cell, both in  $1.5 \text{ M HCl}$  electrolyte at a current density of  $20 \text{ mA cm}^{-2}$  [43].

while the reactions at the negative electrode

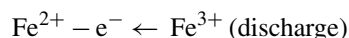


### 3.4. The iron-chromium redox system

This system was one of the first studied. The positive reactant is an aqueous solution of ferric-ferrous redox couple while the negative reactant is a solution of the chromous-chromic couple, both acidified with hydrochloric acid. Their charge and discharge reactions involve simple one-electron transfer as is schematically shown in Fig. 3d and e. At the positive electrode, ferrous iron is transformed to ferric ion

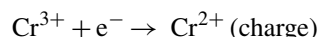


$$E^0 = +0.77 \text{ V versus SHE} \quad (21)$$



$$E^0 = +0.77 \text{ V versus SHE} \quad (22)$$

while at the negative electrode, chromic ions are converted to chromous



$$E^0 = -0.41 \text{ V versus SHE} \quad (23)$$



$$E^0 = -0.41 \text{ V versus SHE} \quad (24)$$

In this redox flow cell the flow rate of each reactant is always higher than the stoichiometric flow requirement, which would result in total reactant utilization in a single pass through the cell. In each cell, an anionic [47] or cationic [48,49] ion exchange membrane separates the two flowing reactant solutions. In an ideal situation the membrane prevents cross diffusion of the iron and chromium ions, permitting free passage of chloride and hydrogen ions for completion of the electrical circuit through the cell. These early cells have been studied by NASA [47,50–59], by a research group of the University of Alicante [48,49,60–66] and by other workers [67].

An investigation of the effect of carbon fibres electrodes on the performance of a Fe–Cr redox flow cell was reported by Shimada et al. [68]. The redox flow cell consisted of two carbon fiber electrodes of  $10 \text{ cm}^2$  geometrical area, separated by a cation exchange membrane. The electrolyte was  $1 \text{ mol dm}^{-3}$  chromic chloride in the negative half-cell and  $1 \text{ mol dm}^{-3}$  of both ferric and ferrous chloride, both in  $4 \text{ N}$  hydrochloric acid in the positive side. It was reported that the coulombic efficiency increased when the structure of the carbon fibers changed from amorphous to graphite and that 95% coulombic efficiency can be maintained if the average space of carbon layer analysed by X-ray was kept under  $0.37 \text{ nm}$ . The authors reported that the

addition of boron into the carbon fibers help to achieve high energy efficiency.

In another study, the Fe–Cr redox system was evaluated using  $1/8 \text{ in.}$  carbon felt electrodes [69]. Since the reduction of chromium is slow in most surfaces, traces of lead ( $100\text{--}200 \mu\text{g cm}^{-2}$ ) and gold ( $12.5 \mu\text{g cm}^{-2}$ ) were deposited on the electrode used for chromium but no catalyst was used for the iron reaction. The area of each electrode was  $14.5 \text{ cm}^2$  and they were separated by an ion exchange membrane (Ionics Inc. series CD1L) the electrolytes were  $1 \text{ mol dm}^{-3}$   $\text{CrCl}_3$  and  $\text{FeCl}_2$  in  $2 \text{ mol dm}^{-3}$   $\text{HCl}$  in the negative and positive sides of the cell, respectively. The open circuit response of this system is shown in Fig. 12 as a function of the percentage of electrolyte charge at a charge/discharge current of  $21.5 \text{ mA cm}^{-2}$ . The curves show that there is a higher polarization during the charging cycle in comparison to the discharge cycle that will cause lower energy storage efficiency. The reason for the different open circuit voltages was attributed to the fact that different chromium complexes predominate during the charge and discharge cycles. Three main chromium species predominate in aqueous  $\text{HCl}$  solutions:  $\text{Cr}(\text{H}_2\text{O})_4\text{Cl}_2^{1+}$ ,  $\text{Cr}(\text{H}_2\text{O})_5\text{Cl}^{2+}$ , and  $\text{Cr}(\text{H}_2\text{O})_6\text{Cl}^{3+}$ . The equilibrium and electrochemical reactions between these complexes is slow but the chromatography and spectrophotometry studies showed that only  $\text{Cr}(\text{H}_2\text{O})_5\text{Cl}^{2+}$  and  $\text{Cr}(\text{H}_2\text{O})_6\text{Cl}^{3+}$  species exist in a discharged solution. During charge the concentration of the  $\text{Cr}(\text{H}_2\text{O})_5\text{Cl}^{2+}$  species decreases faster than  $\text{Cr}(\text{H}_2\text{O})_6\text{Cl}^{3+}$  indicating that this is the chromium species being reduced. During the discharge cycle the concentration of the  $\text{Cr}(\text{H}_2\text{O})_5\text{Cl}^{2+}$  species rises rapidly while the concentration of  $\text{Cr}(\text{H}_2\text{O})_6\text{Cl}^{3+}$  only increases after certain amount of the pentahydrate species has being produced. This shows that the equilibrium between these two species is slow and that their

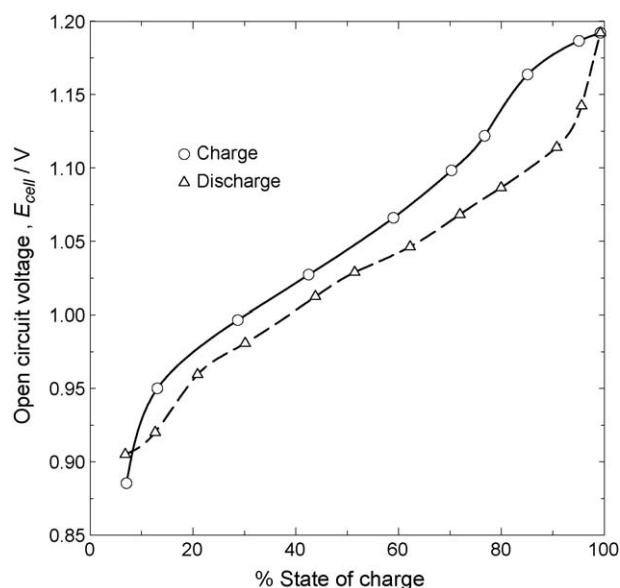
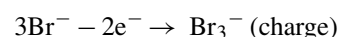


Fig. 12. Open circuit voltage response of an Fe–Cr redox system at  $25^\circ\text{C}$  in  $1 \text{ mol dm}^{-3}$   $\text{CrCl}_3$  and  $1 \text{ mol dm}^{-3}$   $\text{FeCl}_2$  in  $2 \text{ mol dm}^{-3}$   $\text{HCl}$ . Charge/discharge cycles at current density of  $21.5 \text{ mA cm}^{-2}$  and reactant volume to membrane area ratio of  $0.65 \text{ cm}^3 \text{ cm}^{-2}$  [69].

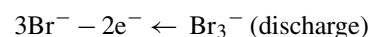
behaviour can be explained in base of their equilibrium potentials.

### 3.5. Zinc/bromine redox flow cells

The zinc/bromine redox flow battery received much interest as a rechargeable power source because of its good energy density, high cell voltage, high degree of reversibility, and abundant, low cost reactants. As in the case of other redox flow cells, the aqueous electrolyte solutions containing reactive species are stored in external tanks and circulated through each cell in the stack. Each cell contains two electrodes at which reversible electrochemical reactions occur. Sometimes, a porous layer or flow-through porous region is used for the bromine electrode. The electrochemical reactions are as follows; at the positive electrode, bromide ions are converted to bromine

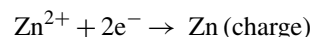


$$E^0 = +1.09 \text{ V versus SHE} \quad (25)$$

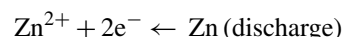


$$E^0 = +1.09 \text{ V versus SHE} \quad (26)$$

At the negative electrode, zinc is reversibly deposited from its ions



$$E^0 = -0.76 \text{ V versus SHE} \quad (27)$$



$$E^0 = -0.76 \text{ V versus SHE} \quad (28)$$

To avoid the reduction of  $\text{Br}_2$  at the zinc electrode during charge, the gap between the positive and the negative electrodes is usually divided by a porous separator. A second liquid phase is circulated with the electrolyte to capture the bromine and further prevent it for reaching the zinc electrode. The organic phase contains complexing agents, such as quaternary ammonium salts, with which the bromine associates to form an emulsion. This emulsion is insoluble in water, has different density than water and travels with the electrolyte to the storage tank where it is separated by gravity.

In order to optimise the zinc/bromine battery, various mathematical models have been used to describe the system [70–73]. The problems with the  $\text{Zn}/\text{Br}_2$  battery include high cost electrodes, material corrosion, dendrite formation during zinc deposition on charge, high self-discharge rates, unsatisfactory energy efficiency and relatively low cycle life. Another disadvantage of this system is that the  $\text{Zn}/\text{Zn}^{2+}$  couple reacts faster than the bromine/bromide couple causing polarization and eventually battery failure. To overcome this, high surface area carbon electrode on the cathode side is normally used however, the active surface area of the carbon eventually decreases and oxidation of the carbon coating occurs.

Despite the drawbacks of this system, a  $\text{Zn}/\text{Br}$  battery with an energy efficiency of 80% has been constructed with two carbon electrodes of  $60 \text{ cm}^2$  and 5 mm interelectrode gap separated by

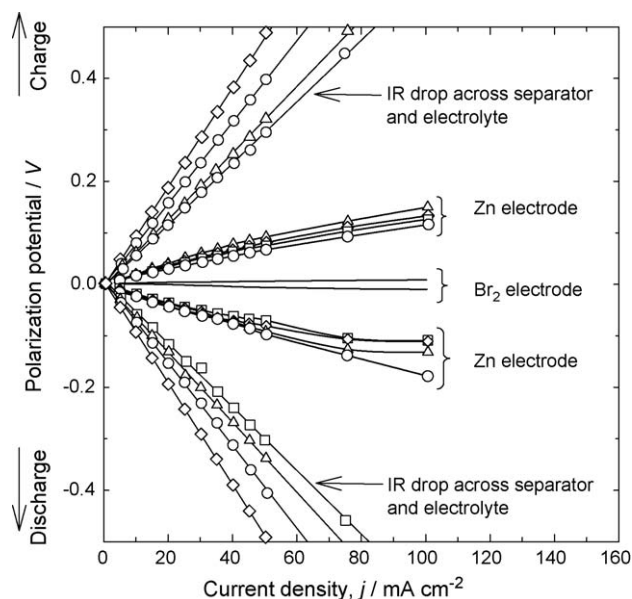


Fig. 13. Cell voltage for Zn and Br electrodes and IR drop across a Nafion® 125 membrane at  $54^\circ\text{C}$  for a  $\text{Zn}/\text{Br}$  battery redox flow cell system at different concentrations of  $\text{ZnBr}_2$ : ( $\diamond$ )  $6 \text{ mol dm}^{-3}$ , ( $\circ$ )  $4 \text{ mol dm}^{-3}$ , ( $\square$ )  $2 \text{ mol dm}^{-3}$  and ( $\triangle$ )  $1 \text{ mol dm}^{-3}$  [74].

a Nafion® 125 or polypropylene microporous membranes [74]. The electrolyte was an aqueous solution of  $1\text{--}7.7 \text{ mol dm}^{-3}$  zinc bromide  $\text{ZnBr}_2$  with an excess of  $\text{Br}_2$  with additives such as potassium or sodium chloride at a flow rate of  $0.5\text{--}3.2 \text{ mL s}^{-1}$ . Initially, the concentration of bromine  $\text{Br}_2$ , in the negative electrode was in excess of  $0.05 \text{ mol dm}^{-3}$  to promote total discharge. The polarization of both electrodes and the potential drop across the separators were measured with a calomel reference electrode; Fig. 13 shows that the polarization of the bromine and zinc electrodes was very low even at charge/discharge current densities above  $100 \text{ mA cm}^{-2}$  and at concentrations of zinc bromide of  $1\text{--}6 \text{ mol dm}^{-3}$ . Most of the potential drop across the cell was due to the IR drop of the electrolyte and the separator as it can be seen from the figure. Zinc dendrites were observed at current densities of  $15 \text{ mA cm}^{-2}$  but they were cut off as they touched the separator without perforate it and hydrogen evolution was observed at this electrode at pH below 3. Fig. 14 shows that constant cell potential is maintained during the charge and discharge cycles followed by sharp potential decrease after ten hours discharge at  $15 \text{ mA cm}^{-2}$  current density. The voltage efficiency was over 80% at a current density of  $30 \text{ mA cm}^{-2}$  but drop just over 45% at  $100 \text{ mA cm}^{-2}$ . This type of battery was proposed for load level applications especially because of its low electrode polarization, low cost, and wide availability of the active materials and electrodes.

### 3.6. Zinc/cerium redox flow cells

This system has been developed by Plurion Systems Inc. [75] and successful operation of a cell at current densities as high as  $400\text{--}500 \text{ mA cm}^{-2}$  has been claimed. The charging reaction is



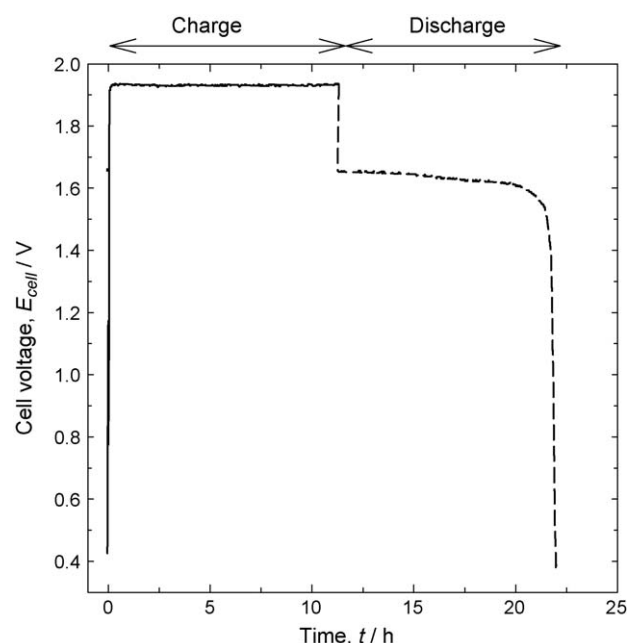


Fig. 14. Charge/discharge response for a Z-Br battery.  $\text{ZnBr}_2$  2 mol  $\text{dm}^{-3}$ ; pH 1.4; current density of 15  $\text{mA cm}^{-2}$  at 25 °C, Nafion® 125 membrane [74].

while the discharging reaction is



The cell voltage of the Zn/Ce system in comparison with other redox systems during charge is approximately 2.5 V and drops below 2 V on the discharge cycle. A Zn/Ce system with a cell containing carbon plastic anodes and platinized titanium mesh cathodes of 100  $\text{cm}^2$  geometrical area separated by a (non-specified type of) Nafion® membrane was patented in 2004 [76]. The gap anode-membrane was 0.4 cm while the cathode-membrane was 0.2 cm with 0.3 mol  $\text{dm}^{-3}$   $\text{Ce}_2(\text{CO}_3)_3$  + 1.3 mol  $\text{dm}^{-3}$  of ZnO in 70 wt.% methanesulfonic acid as anolyte at and 1.3–1.4  $\text{L min}^{-1}$  flow rate. The catholyte consisted of 0.36 mol  $\text{dm}^{-3}$   $\text{Ce}_2(\text{CO}_3)_3$  + 0.9 mol  $\text{dm}^{-3}$  of ZnO in 995 g of methanesulfonic acid at a flow rate of 1.4–1.5  $\text{L min}^{-1}$ , the cell operated at 60 °C. A series of 30 charge/discharge cycles was performed as follows; during 5 min the cell was charged at constant current of 100  $\text{mA cm}^{-2}$  followed by 134 min charge at 50  $\text{mA cm}^{-2}$ . The total charge after this cycle was 1200  $\text{A h m}^{-2}$  (432  $\text{C m}^{-2}$ ). After 1 min rest the cell was discharged at constant voltage of 1.8 V until the current density dropped to 5  $\text{mA cm}^{-2}$ . After 5 min rest, this charge/discharge cycle was repeated 10 times and was followed by similar 20 charge/discharge cycles in which the 50  $\text{mA cm}^{-2}$  charge cycle this time was maintained for 243 min to store a total charge of 2110  $\text{A h m}^{-2}$  (760  $\text{C m}^{-2}$ ) in the cell. Fig. 15 shows the discharge capacity of the cell and the calculated coulombic efficiency during this series of cycles. It can be seen that the coulombic efficiency was larger during cycles when the stored charge was 1200  $\text{A h m}^{-2}$  than when it was 2110  $\text{A h m}^{-2}$ . Also the plot shows that the coulombic efficiency improved slightly in the second series of 30 cycles. Fig. 16 shows the cell voltage during the charge cycle

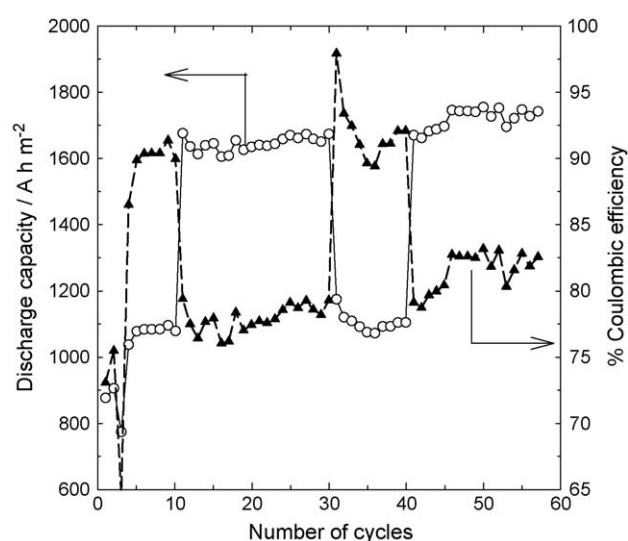
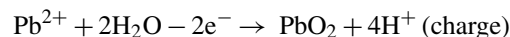


Fig. 15. Discharge capacity and coulombic efficiency for a Zn/Ce redox cell: (○) discharge capacity, and (▲) coulombic efficiency [76].

and the current density during discharge cycle at constant cell voltage of 1.8 V. Both plots were recorded during the 18th cycle.

### 3.7. Soluble lead-acid battery (undivided)

This is a flow battery based on the electrode reactions of lead (II) in methanesulfonic acid. The electrode reactions of the cell shown in Fig. 17 are



$$E^0 = +1.49 \text{ V versus SHE} \quad (31)$$

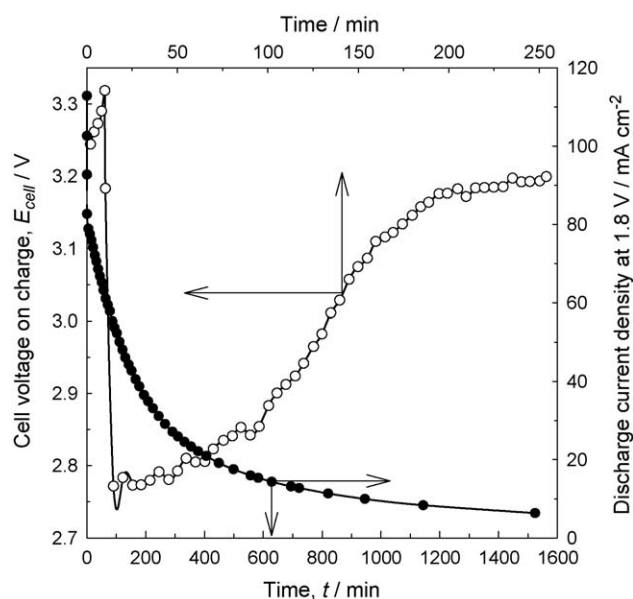


Fig. 16. Voltage during the charge cycle vs. time and discharge current density at constant 1.8 V vs. time for an 18th cycle of a Zn/Ce redox flow cell [76].



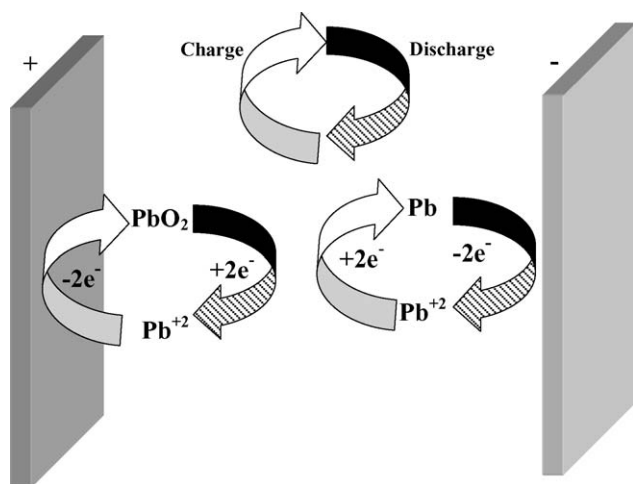
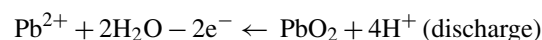
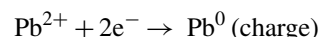


Fig. 17. The concept of a soluble lead-acid acid battery.

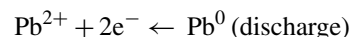


$$E^0 = +1.49 \text{ V versus SHE} \quad (32)$$

negative electrode



$$E^0 = -0.13 \text{ V versus SHE} \quad (33)$$



$$E^0 = -0.13 \text{ V versus SHE} \quad (34)$$

The system differs from the traditional lead-acid battery as Pb(II) is highly soluble in the aqueous acid electrolyte. It also differs from the reported redox flow batteries because only requires a single electrolyte, i.e., no separator or membrane is necessary; this reduces the cost and design complexity of the batteries significantly. The electrode reactions involve the conversion of the soluble species into a solid phase during charging and dissolution at the discharging cycles. This introduces complexities to the electrode reactions and might reduce the performance of the battery if growing metal across the interelectrode gap short circuit the battery. Dissolution and deposition of lead should be fast and no overpotential should be required, however if overpotentials occur hydrogen evolution might take place reducing thus storage capacity.

These cells have been studied in several electrolytes; perchloric acid [77–79], hydrochloric acid, hexafluorosilicic acid, tetrafluoroboric acid [80–83] and most recently in methanesulfonic acid [84–87]. Fig. 18 shows the cell voltage versus time response during the charge/discharge cycles of a soluble lead (II) acid battery in methanesulfonic acid at two current densities [87]. The experiments were carried out in an undivided flow cell containing positive and negative electrodes made of 70 ppi reticulated vitreous carbon and 40 ppi reticulated nickel, respectively. The electrodes were separated by 4 mm interelectrode gap and were prepared by pressing them onto a carbon powder/high density polyethylene back plate current collector of an area of 2 cm<sup>2</sup>. The electrolyte contained 1 g dm<sup>-3</sup> of sodium ligninsulfonate as

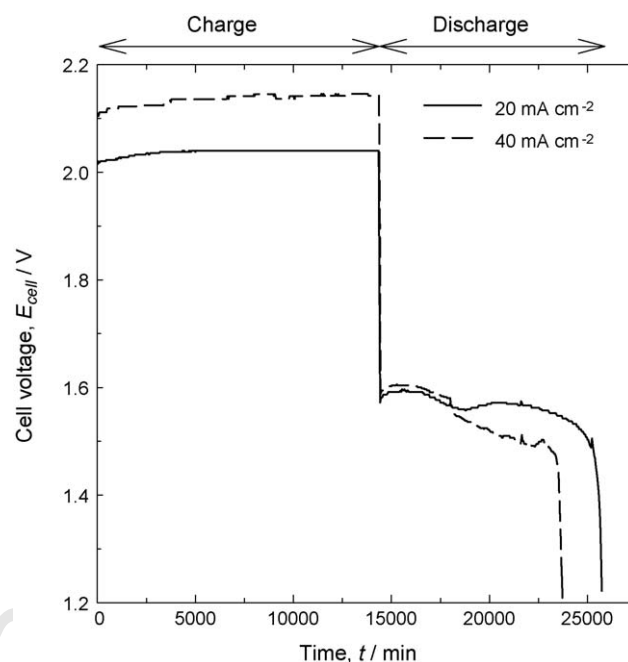


Fig. 18. Cell voltage vs. time for a cell with RVC positive and negative electrodes separated by a 4 mm interelectrode gap in 1.5 mol dm<sup>-3</sup> Pb(CH<sub>3</sub>SO<sub>3</sub>)<sub>2</sub> + 0.9 mol dm<sup>-3</sup> CH<sub>3</sub>SO<sub>3</sub>H + 1 g dm<sup>-3</sup> Ni(II) + 1 g dm<sup>-3</sup> sodium ligninsulfonate. Mean linear flow rate of 10 cm s<sup>-1</sup>. Adapted from Ref. [87].

an additive to decrease the roughness of the lead deposit avoiding the formation of dendrites and to improve the kinetics of the Pb(II)/PbO<sub>2</sub> couple. The curves in the figure show constant voltage during charge and slow voltage drop during the discharge cycles. The overpotential was higher when the applied current was 40 mA cm<sup>-2</sup> in comparison with 20 mA cm<sup>-2</sup>. The charge and energy efficiencies at a current density of 20 mA cm<sup>-2</sup> were 79% and 60% while at 40 mA cm<sup>-2</sup> they were 65% and 46%, respectively. Fig. 19 shows the voltage versus time curves for two sets of 15 min charge/discharge cycles at 20 mA cm<sup>-2</sup>. The low overpotentials observed from the second cycle during the charging process was explained by the formation of insoluble Pb(II) remaining in the positive electrode during the reduction of PbO<sub>2</sub>. During the 79th to the 84th cycles the shape of the curve remains the same but lower overpotentials during the discharge process can be observed.

#### 4. Other characteristics and comparisons

A number of redox flow battery systems are considered in Table 7 (other redox flow cells include: sodium or potassium sulphide-polysulfide species in the anodic reaction and iodide-polyiodide or chloride-chlorine in the cathodic reaction [12], bromine/chromium [88] and uranium [89]). From the systems listed in Table 7, a number of features can be highlighted:

- the size of the cells is generally small with the exception of the bromine/polysulfide system of the Regenesys cells; the installed power is in the range kW for most systems and MW for the bromine/polysulfide system,

Table 7  
Comparison of different redox flow cell systems

| System              | Electrodes                               | Membrane   | $E_{\text{cell}}$ (V) | Current density ( $\text{A m}^{-2}$ ) | Electrode area ( $\text{m}^2$ ) | $R_A$ ( $\Omega \text{m}^2$ ) | Voltage efficiency (%) | Current efficiency (%) | Energy efficiency (%) | Installed power | Installed energy | Temperature ( $^{\circ}\text{C}$ ) | References |
|---------------------|--|--|-----------------------|---------------------------------------|---------------------------------|-------------------------------|------------------------|------------------------|-----------------------|-----------------|------------------|------------------------------------|------------|
| Fe/Cr               | Fe: Carbon felt Cr: Carbon felt+catalyst | Cationic Membrane Nafion® 117 (University of Alicante) | 1.03                  | 9                                     | 0.04                            | $1.1 \times 10^{-1}$          | 81.6                   | 81.2                   | 66.3                  | 10 W            | 80 W h           | 30–55                              | [48,60]    |
|                     |  | Anionic Membrane (NASA Lewis Center)                   | 0.77                  | 64.5                                  | 0.031                           | $1.2 \times 10^{-2}$          | 73                     | 99                     | 72                    | 1 kW            | 10 kW h          | n.a.                               | [48,59]    |
| Bromine/polysulfide | Carbon polymer composite                 | Cationic membrane                                      | 1.54                  | 600                                   | 0.67                            | $2.6 \times 10^{-3}$          | 75                     | 90                     | 67                    | 1, <15 MW       | 120 MW h         | 35                                 | [10]       |
| Vanadium/vanadium   | Graphite felt                            | Selenion CMV   | 1.70                  | 800                                   | 0.15                            | $2.1 \times 10^{-3}$          | 73.2                   | 98.2                   | 71.9                  | 1.33 kW         | 0.7 kW h         | 35                                 | [20]       |
| Soluble lead-acid   | Carbon composite                         | None   | 1.78                  | 100–600                               | 0.0002                          | NG                            | 82                     | 85                     | 65                    | NG              | NG               | 25                                 | [85,86]    |
| Lead-acid           | Lead dioxide and lead                    | Microporous separator                                  | 2.04                  | NG                                    | NG                              | NG                            | NG                     | 80–90                  | 70–75                 | NG              | 6 kW h–24 MW h   | NG                                 | [90]       |

Lead-acid is provided for comparison purposes.

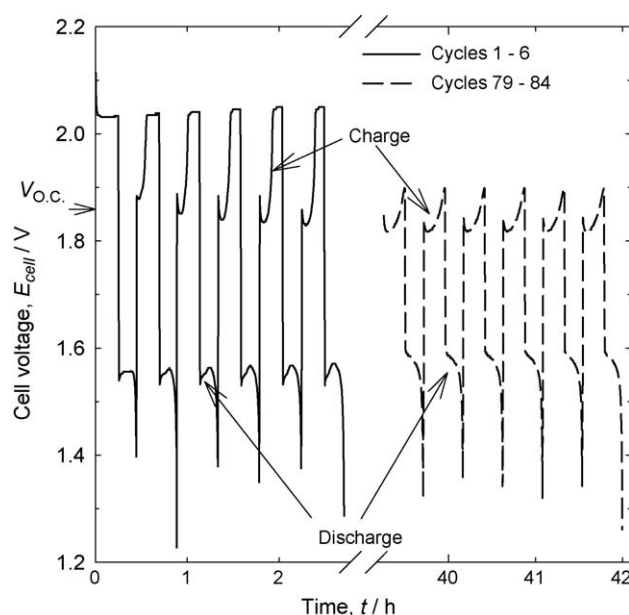


Fig. 19. Voltages vs. time curves for 1–6 and 79–84 charge/discharge cycles at  $20 \text{ mA cm}^{-2}$  during 15 min charge. Cell with Ni foam negative electrode and RVC positive electrode with 4 mm of interelectrode gap in  $1.5 \text{ mol dm}^{-3} \text{ Pb}(\text{CH}_3\text{SO}_3)_2 + 0.9 \text{ mol dm}^{-3} \text{ CH}_3\text{SO}_3\text{H} + 1 \text{ g dm}^{-3} \text{ Ni(II)} + 1 \text{ g dm}^{-3}$  sodium ligninsulfonate. Mean linear flow rate of  $10 \text{ cm s}^{-1}$ . Open circuit potential  $V_{\text{O.C.}}$ , shown in the figure, was 1.86 V. Adapted from Ref. [87].

- (b) the majority of the systems use a cationic membrane to separate the two electrode reactions except the soluble lead-acid battery system,
- (c) most systems use carbon and carbon composite electrodes, three-dimensional and carbon felt electrodes are also used, and
- (d) efficiencies are generally high but are dependent on the state of charge and process conditions, the values are; 73–62% voltage efficiency, 80–98% current efficiency and 66–75% energy efficiency.

The energy density of redox flow batteries in comparison with other battery systems is shown in Fig. 20 [91]; specific energy density of flow cells varies within the range of  $18\text{--}28 \text{ kWh t}^{-1}$  and volumetric energy density within  $21\text{--}35 \text{ kWh t}^{-1}$ . As it is shown in the figure, the energy density of redox flow cells is below the energy density of batteries such as metal-air, lithium-ion,  $\text{Na}_2\text{S}$ , Ni–Cd and lead-acid. These values show that redox flow cells systems can compete with Ni–Cd, super-capacitors, flywheels and lead-acid batteries for energy storage, rather than for portable applications.

As in the case of many batteries, it is important to consider health and safety; many electrolytes require careful manipulation during storage and transport due to their corrosion and toxicity. Another important aspect is the compatibility of the electrolytes; in the case of membrane failure for example, vanadium cells will lose power as the homogeneous reaction will be thermodynamically favourable, however, in other systems the incompatibility of the electrolytes in case of membrane failure can cause more problems and health and safety issues should be considered carefully.

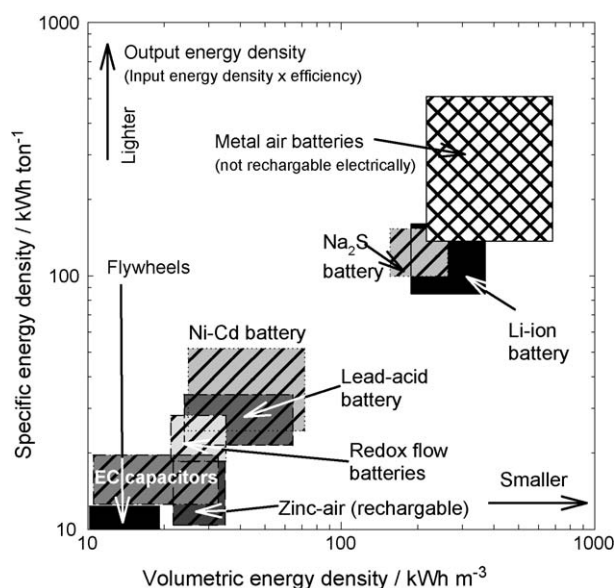


Fig. 20. Specific energy vs. volumetric energy densities for different battery systems [91].

## 5. Summary and further work

Modular technologies such as redox flow systems offer the capability of high power rating; long energy storage time and excellent response time, full power can be delivered in few seconds. Such characteristics are important for better use of power generation in the competitive electricity market. At the generation level, energy storage can be used to increase the load factor of base load and mid merit plant, thereby reducing the need to dispatch less-efficient peaking plant, as well as providing bene-

fits such as meeting load increases and covering operating and contingency reserve.

Electricity transmission companies should be able to increase the load factor of their transmission lines and other assets, while distribution companies can use energy storage to replace or defer investment in generating and other plant, such as static Var compensators, on their electrical network. There is hence, a significant potential market for energy storage products in the range of several hundred MW and several hours storage down to the multi MW level that is presently unsatisfied by existing technology.

Other future markets for these systems are their use in conjunction with renewable energy sources, such as wind power and photovoltaics energy generation systems. A characteristic of renewable sources is their lack of predictable availability at any given time. The redox flow batteries can be used to store energy during periods when conditions favour production, then continuing dispatching the stored electricity at periods of low productivity. In this mode, the redox flow batteries can significantly increase the value of renewable energy sources and represent an efficient energy supply in remote power applications. Table 8 shows some potential applications for redox flow cell storage systems.

The performance of a redox flow cells indicated by the volumetric energy density ( $\text{kWh m}^{-3}$ ) figure of merit, can be enhanced by means of porous, three-dimensional electrodes, highly catalytic electrodes, high linear velocities and good turbulence promoters.

Further work is required in the areas of: (a) reactor characterisation, (b) catalysis by composite (carbon-polymer) electrodes, (c) membrane performance and its effect on electrolyte house-keeping, (d) large scale engineering of redox flow cell systems

Table 8  
Important concepts of the application of redox flow cell storage systems for load levelling

|  |  |
|--|--|
| Generation   |  |
| 1. Spinning reserve  | The generation capacity that a utility holds in reserve, to prevent service interruption in the event of failure of an operating generation station  |
| 2. Generation capacity deferral  | The ability of a utility to postpone installation of new generating facilities by supplementing the existing facilities with an other source   |
| 3. Area/frequency control  | The ability of grid-connected utilities to prevent unplanned transfer of power between themselves and neighbouring utilities (area control) and the ability for isolated utilities to prevent the frequency of the electricity that they produce from deviating too far from a fixed frequency |
| 4. Integration with renewable generation                                       | Integration with renewable generation refers to the renewable power available during peak utility demand   |
| 5. Load levelling  | The storage of inexpensive off-peak power to be dispatched during expensive on-peak hours  |
| 6. Generation dispatch   | The adjustment of the amount of electricity produced by various generation units to the demand. If demand for electricity is higher or below than the electricity produced the generation dispatches decide how to match demand and generation closely   |
| Transmission and distribution  |  |
| 1. Transmission line stability   | The ability to keep all components on a transmission line in synchronisation with each other and prevent system collapse   |
| 2. Voltage regulation  | The ability to maintain the voltages at the generation and load ends of a transmission line within 5% of each other  |
| 3. Transmission facility deferral  | The ability of a utility to postpone installation of new transmission lines and transformers by supplementing the existing facilities with another resource  |
| Customer service   |  |
| 1. Customer demand peak reduction  | The storage of off-peak power for a customer to dispatch during greatest on-peak demand to reduce monthly demand charges   |
| 2. Reliability, power quality, uninterruptible power-small and large customers | The ability to prevent voltage spikes, voltage sags, and power outages that last for a few cycles (less than one second) to minutes from causing data and production loss for customers  |

and their integration with other energy systems and (e) the time-dependence of cell components and their performance. Improvements in redox flow cell technology can be anticipated due to developments in: modular electrochemical reactor and stack design, the engineering of electrode structures, improved electrocatalysis of electrode surfaces, tailoring of the reaction environment in filter-press cells and intelligent control systems to maximise voltage power efficiency.

## References

- [1] DOE, DOE Handbook: Primer on lead-acid storage batteries, DOE-HDBK-1084-95 (1995).
- [2] A. Akhil, S. Swaminathan, R.K. Sen, Cost analysis of energy storage systems for electric utility applications, SANDIA Report, SAND97-0443 UO-1350, 1997.
- [3] Celennium Company Limited, available at: <URL: <http://www.vanadiumbattery.com/page4.html>> (accessed September 27, 2005).
- [4] N.H. Hagedorn, L.H. Thaller, Redox storage systems for solar applications, NASA TM-81464; DOE/NASA/1002-80/5, 1980.
- [5] L.H. Thaller, Electrically rechargeable redox flow cell, US Patent 3,996,064 (December 1976).
- [6] R.E. White, C.W. Walton, H.S. Burney, R.N. Beaver, J. Electrochem. Soc. 133 (1986) 485.
- [7] R.E.W. Jansson, R.J. Marshall, Electrochim. Acta 25 (1982) 823.
- [8] A. Price, S. Bartley, S. Male, G. Cooley, Power Eng. J. 13 (3) (1999) 122.
- [9] P. Morrissey, Int. J. Ambient Energy 21 (4) (2000) 213.
- [10] A. Price, S. Male, M. Kleimaier, VDI Berichte 1734 (2002) 47; F.C. Walsh, Pure Appl Chem. 73 (12) (2001) 1819.
- [11] R. Zito, Process for energy storage and/or power delivery with means for restoring electrolyte balance; US Patent 5,612,148 (March 1997).
- [12] R.J. Remick, P.G.P. Ang, Electrically rechargeable anionically active reduction-oxidation electrical storage supply system; US Patent 4,485,154 (November 1984).
- [13] Regenesys Utility Scale Energy Storage, Project Summary DTI/Pub URN 04/1048, <URL: <http://www.dti.gov.uk/energy/renewables/publications/pubs.distributedgeneration.shtml>> (accessed January 12, 2006).
- [14] D.A. Szánto, Characterization of Electrochemical Filter-Press Reactors, PhD Thesis, University of Portsmouth, UK, 1999.
- [15] P. Zhao, H. Zhang, H. Zhou, B. Yi, Electrochim. Acta 51 (2005) 1091.
- [16] M. Skyllas-Kazacos, M. Rychick, R. Robins, All-vanadium redox battery, US Patent 4,786,567 (November 1988).
- [17] E. Sum, M. Skyllas-Kazacos, J. Power Sources 15 (1985) 179.
- [18] E. Sum, M. Rychick, M. Skyllas-Kazacos, J. Power Sources 16 (1985) 85.
- [19] S. Zhong, M. Kazacos, R.P. Burford, M. Skyllas-Kazacos, J. Power Sources 36 (1991) 29.
- [20] M. Skyllas-Kazacos, D. Kasherman, D.R. Hong, M. Kazacos, J. Power Sources 35 (1991) 399.
- [21] R.L. Largent, M. Skyllas-Kazacos, J. Chieng, Improved PV system performance using vanadium batteries, in: Proceedings of the IEEE 23rd Photovoltaic Specialists Conference, Louisville, Kentucky, May, 1993.
- [22] C. Menictas, D.R. Hong, M. Kazacos, M. Skyllas-Kazacos, Vanadium battery solar demonstration house, in: Proceedings of the Solar '94 Conference, vol. 2, Sydney, Australia, 1994, p. 611.
- [23] C. Menictas, D.R. Hong, Z.H. Yan, J. Wilson, M. Kazacos, M. Skyllas-Kazacos, Status of the vanadium redox battery development program, in: Proceedings of the Electrical Engineering Congress, vol. 1, Sydney, Australia, 1994, p. 299.
- [24] C. Menictas, T. Tran, M. Skyllas-Kazacos, The dissolution of  $V_2O_5$  in vanadium sulphate solution, in: Proceedings of the Ninth Australasian Electrochemistry Conference, vol. 2, Wollongong, Australia, 1994, p. 66.
- [25] M. Kazacos, M. Skyllas-Kazacos, J. Electrochem. Soc. 136 (1989) 2759.
- [26] V. Haddadi-Asl, M. Kazacos, M. Skyllas-Kazacos, J. Appl. Electrochem. 25 (1995) 29.
- [27] C. Menictas, D.R. Hong, M. Kazacos, M. Skyllas-Kazacos Vanadium back up battery for submarine application, Final Report, Australian Defence Dept., October 1995, p. 120.
- [28] C. Menictas, M. Skyllas-Kazacos, Vanadium/oxygen redox fuel cell; Final Report to NSW Office of Energy, State Energy Research and Development Fund, April, 1997.
- [29] M. Skyllas-Kazacos, M. Kazacos, High energy density vanadium electrolyte solutions for all-vanadium redox battery, International Patent Application No. PCT/AU96/00268, May, 1996.
- [30] M. Skyllas-Kazacos, F. Grossmith, J. Electrochem. Soc. 134 (1987) 2950.
- [31] C. Menictas, M. Cheng, M. Skyllas-Kazacos, J. Power Sources 45 (1993) 43.
- [32] S.C. Chieng, M. Kazacos, M. Skyllas-Kazacos, J. Power Sources 39 (1992) 11.
- [33] S. Zhong, C. Padeste, M. Kazacos, M. Skyllas-Kazacos, J. Power Sources 45 (1993) 29.
- [34] M. Skyllas-Kazacos, D. Kasherman, D.R. Hong, M. Kazacos, J. Power Sources 35 (1991) 399.
- [35] S. Zhong, M. Skyllas-Kazacos, J. Power Sources 39 (1992) 1.
- [36] M. Skyllas-Kazacos, C. Menictas, M. Kazacos, J. Electrochem. Soc. 143 (1996) L86.
- [37] T. Mohammadi, M. Skyllas-Kazacos, J. Power Sources 63 (1996) 179.
- [38] T. Mohammadi, M. Skyllas-Kazacos, J. Appl. Electrochem. 27 (1997) 153.
- [39] T. Mohammadi, S.C. Chieng, M. Skyllas-Kazacos, J. Membr. Sci. 133 (1997) 151.
- [40] The vanadium redox battery, <URL: <http://www.ceic.unsw.edu.au/centers/vrb>> (accessed September 27, 2005).
- [41] Sumitomo Electric, <URL: <http://www.sei.co.jp/index.en.html>> (accessed September 27, 2005).
- [42] R. Ferringo, A.D. Stroock, T.D. Clark, M. Mayer, G.M. Whitesides, J. Am. Chem. Soc. 124 (2002) 12930.
- [43] M. Skyllas-Kazacos, J. Power Sources 124 (2003) 299.
- [44] M. Skyllas-Kazacos, A. Mousa, M. Kazacos, Metal bromide redox flow cell, PCT Application, PCT/GB2003/001757, April, 2003.
- [45] M. Skyllas-Kazacos, Y. Limantari, J. Appl. Electrochem. 34 (2004) 681.
- [46] M. Skyllas-Kazacos, J. Power Sources 124 (2003) 299.
- [47] R.B. Hodgdon, W.A. Waite, S.S. Alexander, Anion permselective membrane, NASA CR-174725, DOE/NASA/0264-1, 1984.
- [48] P. Garces, M.A. Climent, A. Aldaz, An. Quim. 83 (1987) 9.
- [49] M.A. Climent, P. Garces, M. Lopez-Segura, A. Aldaz, An. Quim. 83 (1987) 12.
- [50] N.H. Hagedorn, L.H. Thaller, Design flexibility of redox flow systems NASA TM-82854, DOE/NASA/12726-16, 1982.
- [51] L.H. Thaller, Electrically rechargeable redox flow cells, NASA TM-X-71540, 1974.
- [52] L.H. Thaller, Redox flow cell energy storage systems; NASA TM-79143, DOE/NASA/1002-79/3, 1979.
- [53] L. Swette, V. Jalan, Development of electrodes for the NASA iron/chromium redox system and factors affecting their performance, NASA CR-174724, DOE/NASA/0262-1, 1984.
- [54] M.A. Hoberecht, L.H. Thaller, Performance mapping studies in redox flow cells, NASA TM-82707, DOE/NASA/12726-13, 1981.
- [55] N. Hagedorn, M.A. Hoberecht, L.H. Thaller, NASA redox cell stack shunt current, pumping power, and cell performance tradeoffs, NASA TM-82686, DOE/NASA/12726-11, 1982.
- [56] D.A. Johnson, M.A. Reid, Chemical and electrochemical behaviour of the Cr(III)/Cr(II) half cell in the NASA redox energy storage system, NASA TM-82913, DOE/NASA/12726-17, 1982.
- [57] L.H. Thaller, Recent advances in redox flow cell storage systems, NASA TM-79186, DOE/NASA/1002-79/4, 1979.
- [58] R.F. Gahn, N.H. Hagedorn, J.A. Johnson, Cycling performance of the iron-chromium redox energy storage system, NASA TM-87034, NASA, Dept. of Energy, US, 1985.



- [59] N.H. Hagedorn, NASA redox storage system development project, NASA TM-83677, DOE/NASA/12726-24, 1984.
- [60] G. Codina, J.R. Perez, M. Lopez-Atalaya, J.L. Vazquez, A. Aldaz, J. Power Sources 48 (1994) 293.
- [61] G. Codina, A. Aldaz, J. Appl. Electrochem. 22 (1992) 668.
- [62] G. Codina, M. Lopez-Atalaya, J.R. Perez, J.L. Vazquez, A. Aldaz, Energía March–April (1990).
- [63] G. Codina, M. López-Atalaya, J.L. Vázquez, A. Aldaz, P. Garcés, Bull. Electrochem. 5 (1989) 645.
- [64] M. López de Atalaya, G. Codina, J.R. Pérez, M.A. Climent, J.L. Vázquez, A. Aldaz, J. Power Sources 35 (1991) 225.
- [65] J.R. Pérez, M. López-Atalaya, G. Codina, J.L. Vázquez, A. Aldaz, Bull. Electrochem. 7 (1992) 555.
- [66] M. López-Atalaya, G. Codina, J.R. Pérez, J.L. Vázquez, A. Aldaz, J. Power Sources 39 (1992) 147.
- [67] C.Y. Yang, J. Appl. Electrochem. 12 (1982) 425.
- [68] M. Shimada, Y. Tsuzuki, Y. Iizuka, M. Inoue, Chem. Ind. 3 (1988) 80.
- [69] D.A. Johnson, M.A. Reid, J. Electrochem. Soc. 132 (1985) 1058.
- [70] T.I. Evans, R.E. White, J. Electrochem. Soc. 134 (1987) 866.
- [71] G.D. Simpson, R.E. White, J. Electrochem. Soc. 136 (1989) 2137.
- [72] G.D. Simpson, R.E. White, J. Electrochem. Soc. 137 (1990) 1843.
- [73] T.I. Evans, R.E. White, J. Electrochem. Soc. 134 (1989) 2725.
- [74] H.S. Lim, A.M. Lackner, Knechtli, J. Electrochem. Soc. 124 (1977) 1154.
- [75] High Capacity Electrical Storage & Power Conditioning Units, Available at: <URL: <http://plurionsystems.com>> (accessed September 27, 2005).
- [76] R.L. Clarke, B.J. Dougherty, S. Harrison, J.P. Millington, *Battery with bifunctional electrolyte*. United States Patent Application, International publication number: WO 2004/095602 A2, November 4, 2004.
- [77] J.P. Schrodt, W.T. Otting, J.O. Schoegler, D.N. Craig, Trans. Electrochem. Soc. 90 (1946) 405.
- [78] J.C. White, W.H. Powers, R.L. McMurtric, R.T. Pierce, Trans. Electrochem. Soc. 91 (1947) 1947.
- [79] G.D. McDonald, E.Y. Weissman, T.S. Roemer, J. Electrochem. Soc. 119 (1972) 660.
- [80] F. Beck, US Patent 4,001,037 (1977).
- [81] R. Wurmb, F. Beck, K. Boehlke, US Patent 4,092,463 (1978).
- [82] P.O. Henk, Z.A.A. Piontkowski, US Patent 4,331,744 (1982).
- [83] P.O. Henk, US Patent 4,400,449 (1983).
- [84] A. Hazza, D. Pletcher, R. Wills, Phys. Chem. Chem. Phys. 6 (2004) 1773.
- [85] D. Pletcher, R. Wills, Phys. Chem. Chem. Phys. 6 (2004) 1779.
- [86] D. Pletcher, R. Wills, J. Power Sources 149 (2005) 96.
- [87] A. Hazza, D. Pletcher, R. Wills, J. Power Sources 149 (2005) 103.
- [88] J.D. Giner, H.H. Stark, Redox battery including a bromine positive electrode and a chromium ion negative electrode and method, US Patent 4,469,760 (September 1984).
- [89] T. Yamamura, Y. Shiokawa, H. Yamana, H. Moriyama, Electrochim. Acta 48 (2002) 43.
- [90] D. Linden, Handbook of Batteries and Fuel Cells, McGraw Hill, New York, 1984.
- [91] Electricity Storage Association <URL: <http://www.electricitystorage.org>> (accessed January 28, 2006).